ELSEVIER

Contents lists available at ScienceDirect

Manufacturing Letters

journal homepage: www.elsevier.com/locate/mfglet



Letters

Characterizing process window for microscale selective laser sintering



Dipankar Behera, Aaron Liao, Michael A. Cullinan*

Walker Department of Mechanical Engineering, The University of Texas at Austin, 204 E Dean Keeton St, Austin 78712, USA

ARTICLE INFO

Article history: Received 28 February 2023 Received in revised form 20 May 2023 Accepted 26 June 2023 Available online 9 July 2023

Keywords:
Microscale laser additive manufacturing
Sintering window
Metal nanoparticle sintering

ABSTRACT

This paper outlines the experimental approach to create a sintering window for a microscale metal additive manufacturing (AM) process. The experimental framework discussed in the paper involves fabricating sintered features by varying pattern area and laser irradiance. The sintered features are then imaged under a microscope and the processed images are compared against an ideal image to quantify the uncertainty in near-net shape of the feature. Evaluating this data defines the process window within which good sintering and near-net shaped features can be expected in the microscale AM process.

© 2023 Published by Elsevier Ltd on behalf of Society of Manufacturing Engineers (SME).

1. Introduction

Additive manufacturing (AM) technologies have im-proved the functionality and manufacturability of compo-nents in an unparalleled manner. [1] Colloquially known as 3D printing, AM systems have grown from being low-volume, rapid prototyping installations to integral parts of mass production and assembly lines. Although convention-ally, additive manufacturing is a layer-bylayer fabrication process, there has also been a significant pushed towards volumetric fabrication (where the feature dimensions can be simultaneously discretized in all three axes), with the advent of new materials, processing and image projection techniques [2]. Compared to conventional subtractive manu-facturing processes, the fabrication freedom available using AM technologies has also opened up the design space to focus more on optimized structural, thermal and ergonomic characteristics of the design in addition to cost and manu-facturability. Several industries are vertically integrating the hardware, software and services needed to create a robust AM infrastructure. AM technologies such as powder bed fusion (PBF) techniques and vat photopolymerization have gradually transformed from rapid prototyping technologies restricted for design exploration to mainstream fabrication methods for production scale manufacturing, primarily in the aerospace, automotive and defense sectors. AM has also led to the development of novel medical devices, and has assisted development of complex medical procedures with several leading AM capital

E-mail address: Michael.Cullinan@austin.utexas.edu (M.A. Cullinan).

equipment companies partner-ing with medical experts to develop solutions to visualize and assist medical professionals and hospitals in complex surgeries.

However, the design freedom associated with AM tech-nologies has not been leveraged for fabricating micro/nano-scale features with potential applications in semiconductor packaging, micro-scale electro/optoelectronic mechanical devices (MEMS/MOEMS), and microscale medical devices to name a few. Most commercially available metal AM machines are only able to fabricate down to 100 m feature sizes, and are also limited by low throughput which makes them incompatible with these industries.

The challenges associated with scalability of existing AM technologies and current needs of the semiconductor packaging industry demands exploration of novel microscale AM technologies to address these challenges and introduce new design rules which might simplify fabrication of pre-viously infeasible designs. This paper discusses an exper-imental framework developed to characterize the sintering window for a microscale metal AM technology. In this paper, the effect of key variables such as laser irradiance, feature area, exposure duration/number of bursts have been used as the experimental variables to outline a process window within which near-net shaped features can be fabricated.

2. Motivation behind this work

Microscale selective laser sintering (-SLS) is a mi-croscale PBF technique that can fabricate true three-dimensional metal structures with a feature-size resolution of 5 m [3]. This process has primary applications in the microelec-tronics packaging industry due to its desirable throughput over large areas and ability to create pillar-like structures with high aspect ratios which it accomplishes

^{*} Corresponding author.

in a layer-by-layer manner. The -SLS process operates similarly to traditional selective laser sintering processes (SLS) except that the powders used are at the nanoscale and are suspended in a dispersion instead of microparticles in a powder bed.

In addition, a digital micromirror device (DMD) is used to spatially modulate the laser and selectively heat regions of the powder bed instead of a raster scan.

Minimum feature size in current commercially available macroscale metal PBF processes is limited to 50 m [4]. To expand the application of metal additive manufacturing to industries such as MEMS or semiconductor packaging, line widths of at least 40 m are required. To achieve features at this scale, nanoscale particles must be used. However, nanoparticles agglomerate due to van der Waals forces which leads to poor spreadability during repeated powder layer deposition, making them incompatible with traditional PBF processes. Additionally, due to their high surface area. oxidation occurs rapidly in the metal nanoparticles, making them more difficult to sinter in an open environment. To address these issues in microscale SLS, nanoparticles are be suspended in a dispersion with diethylene glycol (DEG) which prevents agglomeration and reduces oxidation. Thus, the significant difference between the sintering properties of nanoparticle inks used in -SLS and powders used in macroscale metal AM presents a need for thorough analysis and optimization of sintering parameters. Further details about the setup and system-level design and validation of the -SLS tool can be found in reference [3].

Processing temperatures for PBF techniques vary due of the many different materials and characteristics of the powder used for the fabrication process. In general, sintering windows for each material and process are established to ensure the particles fuse while minimizing undesired effects caused by exceeding the optimal temperature range. A commonly used technique to estimate these temperature windows in polymer PBF processes is differential scan-ning calorimetry (DSC). It can be used to characterize any polymer powders used and determine the temperature windows at which thermally induced defects are minimized [5]. The temperature window for metal PBF processes can be determined with the melting temperature of the material used, however determining laser parameters is much more difficult as it involves controlling melt pool dynamics caused from temperature gradients within the molten material [6].

In direct metal laser melting (DMLM), a macroscale PBF process, mass transfer between microscale particles pri-marily occurs through melting. Melt pool dynamics caused by the physics of wetting, convection, surface tension, recoil pressure near the heated area must be considered to optimize part properties and dimensional accuracy. In contrast, the -SLS uses particles on the nanoscale which allow for sintering well below the melting temperature of the bulk material [7]. At these temperatures, the mass transfer occurs through grain boundary and surface diffusion instead of melting. Because of this, controlling the temperature gradients outside of the exposed laser area is a critical challenge to improving dimensional accuracy of the -SLS process. These gradients can be large enough to produce fully or partially sintered regions outside of the exposed area, leading to reduction in part resolution. Optimization of laser heating parameters to determine the sintering window will reduce residual stresses and help achieve near net shape parts. Previous investigations of sintering of nanoparticle inks with the -SLS process were concerned with evaluating the morphology of sintered material with varying laser irradiance and ink layer [7].

This study focuses on the deviation between the laser exposure area and sintered part area across varying laser irradiance and spot size. The effects of exposure duration and spatial modulation with the digital micromirror device (DMD) have not yet been thoroughly explored, and it is necessary to verify the models developed

for the prediction of heat transfer during the sintering process. Understanding of the sintering window will also aid in the development of -SLS to materials beyond copper and silver.

3. Characterizing sintering window

3.1. Discussion of the procedure

The -SLS process uses digital masks using a DMD to achieve single layer and multilayer sintering of nanoparti-cle inks using an 808 nm CW laser (DILAS IS39 series multimode fiber, 808 nm wavelength, water cooled diode laser with quasi-CW (QCW) option). However, the optimal operating window where good sintering with near net shaped parts could be achieved is not known. Therefore, primary objective of this study is to characterize the sintering win-dow for the laser-material interaction with varying process parameters. The material used in this study is a commercially available silver nanoparticle ink formulation (Novacentrix IS-A102A, 40% w/w Ag, 30–50 nm average particle size distribution). The substrate used in this study is a 1 mm thick borosilicate glass slide. The key parameters affecting the total irradiance on the substrate are the laser floating voltage, current, number of bursts, pulse width and pulse repetition rates (corresponds to the duty cycle). Due to the large number of variables involved, the design of experiment (DOE) space was reduced by operating the laser at a 10% duty cycle with pulse width and pulse repetition rates at 1 ms and 100 Hz respectively. Another key variable involved in this study is the number of pixels that are'on'. The DMD used for the study has a total of 1920×1080 pixels. Each pixel in the DMD is 7.6 m \times 7.6 m. A set of focusing and collimating optics is used in the -SLS setup to obtain a diffraction limited spot size resolution of approximately 1.2 m \times 1.2 m which equals 2.4 mm \times 1.3 mm area on the nanoparticle bed when all the micromirrors are'on' [3]. The largest square corresponds to a total of 1080×1080 pixels that can be turned'on'. For the purposes of this study, this is classified as a 100% square or S1. Similarly, S2 corresponds to a 75% square, S3 corresponds to a 50% square, S4 corresponds to a 25% square and S5 corresponds to a 10% square. Based on these definitions, the range of parameters for the combined DOE space is shown in Table 1.

As shown in Table 1, the square pattern area was varied to prepare samples with varying areas. However, it is important to note that there are spatial and temporal losses asso-ciated with the switching DMDs, which changes the overall output intensity profile of the micromirror array. This would also affect the near-net shape part characteristics and the heat affected zones. The parameter ranges were chosen with the following considerations — 1. Maximum drive current for the laser (55 A max), 2. Number of bursts were chosen based on the maximum burst and duty cycle limitations of the laser driver (Analog Module 8800D) without over heating the laser, 3. The different square dimensions were chosen to study the effect of number of pixels (or spots that are being heated).

The laser was operated at the input parameters shown in Table 1 and the substrate was scanned over a 10 mm \times 10 area to obtain the repeatable instances of the different patterns. Next, the squares

Table 1Sintering window parameters and ranges.

Parameter	Value	Units
Floating Voltage	17, 18, 19, 20	V
Input Current	20, 25, 30, 40, 50	Α
Number of Bursts	10-250	
Square area	100, 75, 50, 25, 10	%

are profiled and measured with the laser confocal microscope (Keyence VKX-1100) using its *step*, *scan and stitch* functionalities to get high-resolution images. The obtained image was processed to account for plane tilt and centered with respect to a reference image to simplify further analyses. Next, the digital image is seg-

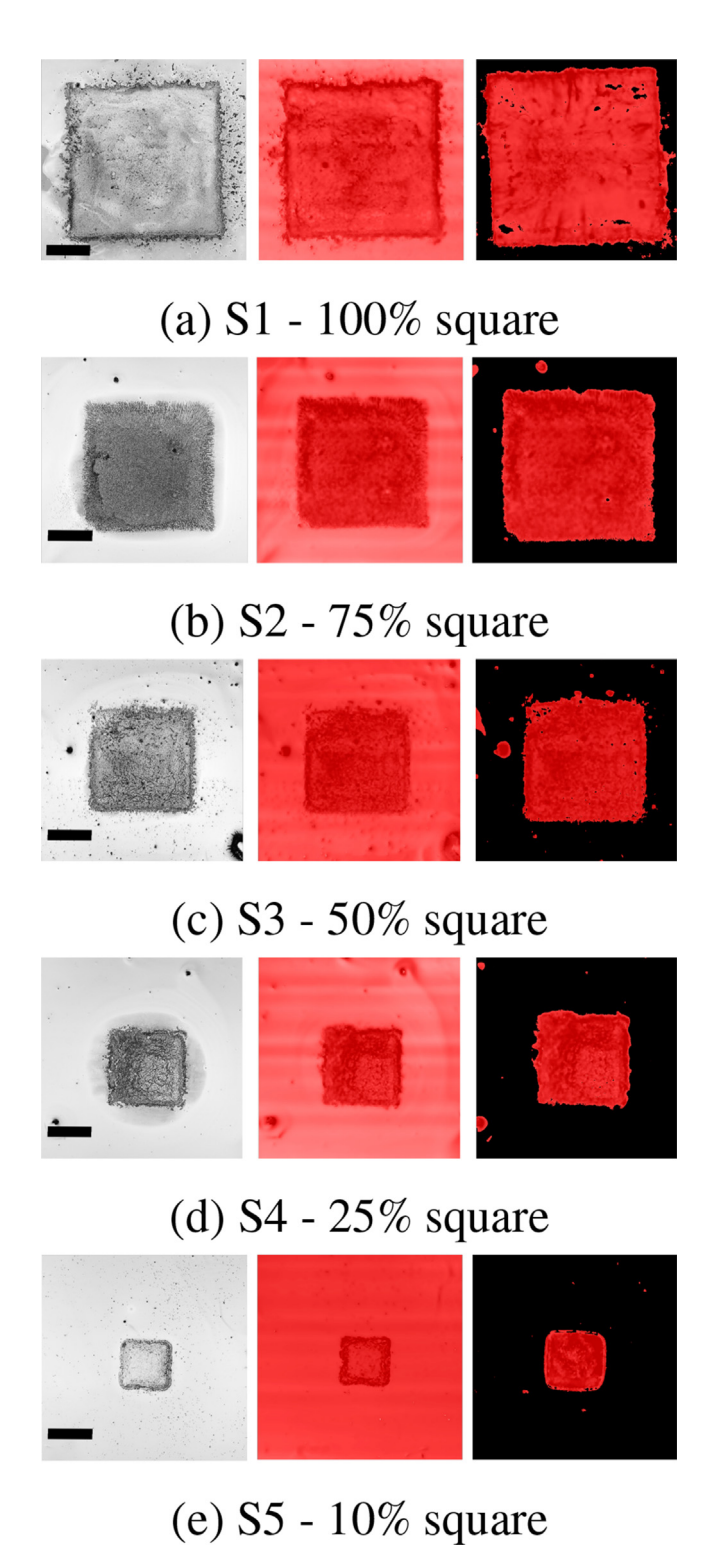


Fig. 1. [Scale bar = 125 m] Figure showing the optical image and laser confocal image (after processing) in the first two columns as obtained from the profilometer. Column 3 shows the image processed and segmented using the K-means clustering algorithm. All the images shown here correspond to the *'good sintering'* region presented in the final sintering window in Fig. 3.

mented into two distinct regions with superpixels of similar attributes. Due to random fluctuations in heights, the profilometer images had unwanted contrast as seen in the grayscale images of Fig. 1a and 1e. The peaks formed at the edges due to the coffeering effect meant that the data did not have clearly defined labels which could be used to distinguish and identify the edges of the squares reliably. Using the MultiFile Analyzer software, the image was further processed to remove and smooth out the noise due to random particles and debris.

The image data was converted to a monochromatic grayscale to reduce the number of clusters. During the image segmentation process, pixels with similar characteristics are assigned a label and clustered to form a composite. The K-means clustering algorithm was chosen to segment the image. K-means is an unsupervised learning approach that is used to outline the desired area by clustering images with similar intensities into'k' number of partitions. The basic objective function of this algorithm is to minimize the sum of squared distance between the points in a cluster and the centroid of the cluster. In this case, first image was subdivided into into multiple images (ranging from 2 to 5) and then morphed to get rid of the clusters with noise. Fig. 1, shows the segmentation process in action for the different areas of images processed. It must be noted that the ink was completely dried using a hot plate at 85 °C to avoid any artifacts due to improper/partial drying.

The pixels were scaled based on the dimensions obtained from the optical profilometer data of the samples. This was used to calculate the area of the final image cluster. Matlab's batch processing tool was used to apply this approach to around 90 images. However, as it can be seen in Fig. 1, there were still some unwanted features around the edges and in the center of the square that were not filtered out by the clustering algorithm.

In the context of the study, *good sintering* is considered if the sintered part area and shape is similar and within 10% of the desired part area and shape. Additionally, in a previous work by Roy et al, scanning electron microscope images show that sintered area of a part has necking between the nanoparticles which undergo solid-state diffusion after during the thermal cycle as compared to seeing individual nanoparticles in the unsintered area [8]. The unsintered nanoparticle ink has poor adhesion to the substrate and is either washed off or dried (at temperatures below sintering temperature of 140 °C prior to analyzing the images in this study. Hence, the regions of interest analyzed in this study are sintered.

3.2. Results

The power and irradiances corresponding to each sin-tered sample were measured using a thermopile photode-tector (Ophir 10A) with a 50 kW/cm² damage threshold. In Figs. 2, 5 subplots are shown which outline the sintering window based on the power measurements using the pho-todetector, and the image processing of the different optical images as discussed in the previous section. Fig. 2 a-e show the measured power for different bursts and current values. As expected, the increasing number of bursts show a linear trend and the slope becomes steeper with increasing current values. The'good' sintering window is defined as the region where the absolute error between the measured square area and the ideal square area is within 10% and is shown by the red/shaded area in all the plots. An example of parts which fell outside the bounds of bounds of the 10% cutoff area is show in Appendix 1, Fig. 5.

An error of 100% denotes that there were no sintered features observed at those parameters. For the 100% square (Fig. 2a), good sintering is not observed for 20A or 25A at the given number of bursts. Beyond 30A, 20 bursts the near-net shape of the sintered features is closer to the projected geometry and hence falls under

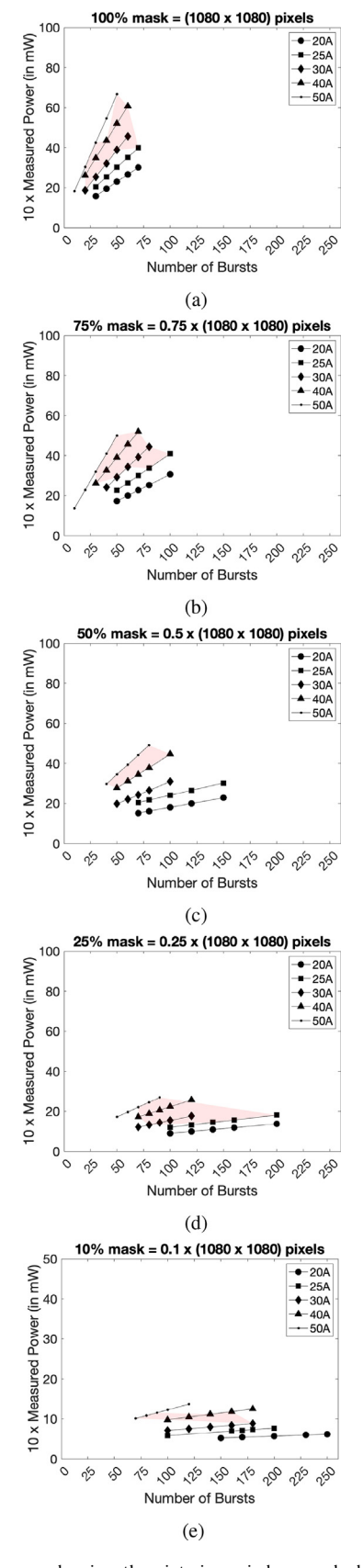


Fig. 2. Set of figures showing the sintering windows and absolute errors in measured areas for varying current and burst configurations. The light red zone is defined as a good sintering window which is the set of the points for which the measured area error is less than $10\,\%$. The subplots show Power (mW) vs Number of Bursts for (a) S1 – $100\,\%$ mask (b) S2 – $75\,\%$ mask (c) S3 – $50\,\%$ mask (d) S4 – $25\,\%$ mask (e) S5 – $10\,\%$ mask. (For interpretation of the references to color in this figure legend, the reader is referred to the web version of this article.)

the good sintering region. The outlier at 50A, 50 bursts corresponds to a larger square with HAZ. For the 75% square area (Fig. 2b), at 20A drive current and 100 bursts, the minimum geometry error is at 40% which is characterized by a smaller geometry. In this case, good sintering can be seen to start at 25A, 80 bursts. Similarly, for other regions, the required bursts corresponding to the drive current can be observed. However, there are some outliers ((Fig. 2a) 40A,60 bursts), which are due to a combination of clustering errors, excessive splashing/distortion of geometry during sintering or presence of dust particles during measurement. These outliers can be effectively removed by repeating the tests. For a 50% square(Fig. 2c), good sintering can only be observed above 40A within 120 bursts. Therefore, for the 25% and 10% squares, higher burst counts were used. However, as it can be seen in Figure (Fig. 2d) and (Fig. 2e), at higher bursts, the errors started increasing (at 40A and 50A specifically), indicating that the sintered features were getting larger with higher heat affected zones. As seen in Fig. 2e, the sintering window for a smaller area seems to be narrower than the previous ones, with a less steep power vs bursts line. A small increment the irradiance for this pattern leads to higher HAZs seen at the outliers (e.g. 50A, 120 bursts). Additionally, the thin sintering zone seen in (Fig. 2e) means that the sintering window for near net shaped parts must be pre-determined and validated (using thermal simulation models validated using similar experi-ments), without which higher HAZs would be imminent. Fig. 3 shows the consolidated sintering window for the experimental space and highlights the regions which show insufficient sintering (sintered feature area < pattern area) and heat affected zones (sintered feature area > pattern area).

To get a better understanding of the combined sinter-ing window across the entire design space, the irradiance (W/cm²) versus absolute error in the measured area (%) was plotted. As shown in Fig. 3, different color dots correspond to sintering for squares of different areas - S1 corresponds to 100%, S2 corresponds to 75% and so on. The darker dots show the data points where good sintering can be seen. The irradiance vs error plots follow an power law fit with the coefficients as shown in Table 2. It is interesting to note that there are several outliers (absolute error > 10%) for the same irradiance band. As the irradiance increases, parts with higher HAZs are formed and hence the deviation from the original mask dimension also increases. Within the design space presented in this study, this trend is clearly seen for smaller sintered features,

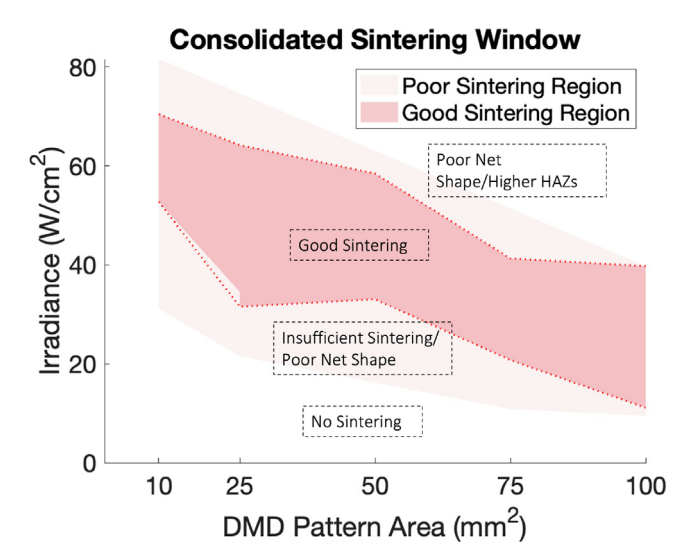


Fig. 3. Consolidated sintering window outlining the ir-radiance and pattern area for insufficient sintering, good sintering and poor net shape due to formation of heat affected zones.

Table 2Coefficients for the sintering normalized sintering window for an exponential fit (() = +) within 95% confidence interval bounds.

Square Area	Α	В	С
(%)			
100 (S1)	187.1	-0.26	-70.28
75 (S2)	391.2	-0.39	-91.13
50 (S3)	1.91x10 ⁶	-3.27	1.97
25 (S4)	2.21×10^{15}	-9.49	12.37
10 (S5)	9.19×10^{9}	-5.187	7.56

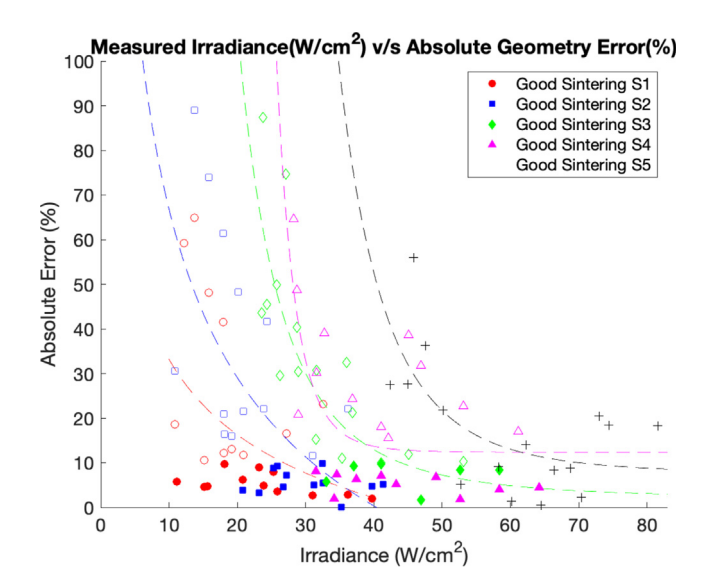


Fig. 4. Measured Irradiance v/s Absolute error as obtained for different squares (S1 - 100%, S2 - 75 %, S3 - 50 %, S4 - 25 %, S5 - 10 %.

e.g. S4 (25% square) and S5 (10% square). Therefore, effective sintering window can be completely defined by considering the points in Figs. 3 and 2.

For the input parameters considered in these experi-ments, at low irradiances due to lower currents or bursts, the material is not exposed to sufficiently high and uniform thermal gradients, thereby leading to a smaller than desired features. It was also seen that the error between the part formed and the desired part increased as the irradiance increased. This was primarily because of higher HAZs being formed. For smaller desired areas (part sizes), this effect was more pronounced as seen in Fig. 4. For larger parts, exposing the laser for longer durations led to the cracking of the glass slide due to localized thermal stresses. Ideally, it can be hypothesized that if the micromirrors had a much higher damage thresholds and the substrate had better frac-ture strength, similar increase in HAZs could be observed for larger parts as well. These experiments show that the window for'good' sintering reduces as the part size goes down, primarily because at higher irradiances over smaller spot sizes leads to larger HAZs.

4. Conclusion

Microscale additive manufacturing is gathering signifi-cant interest within the additive manufacturing community. It opens up a plethora of new applications with miniaturized and high precision parts that can complement or effectively replace their lithographic analogs, especially in the semiconductor industry. The -SLS system developed by the authors can fabricate microscale metal parts which are otherwise difficult to handle and process at these scales using conventional metal AM approaches. This work

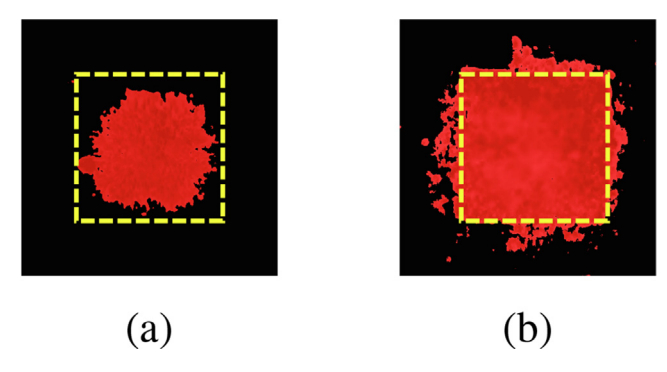


Fig. 5. Examples of squares that do not fall within the 10% cutoff. Dotted yellow line shows an ideal 25 % square with a 0.419 mm² area (a) Insufficient sintering (b) Extra sintering with heat affected zones. (For interpretation of the references to color in this figure legend, the reader is referred to the web version of this article.)

involves a detailed experimental study of the -SLS process using off-the-shelf image processing tools to understand the impact laser processing parameters and input feature sizes on the near-net shape of the printed part.

This paper presents the sintering window for varying laser powers and projected pattern size. As expected, the power increases with an increase in the current and number of bursts, and an analysis of parts fabricated under the con-ditions shown in the plots helps in generating the sintering window for a specific pattern size. The irradiance versus pattern area plot shows the band where good sintering can be expected and is slightly narrower for smaller pattern area (Fig. 3). This is primarily because at smaller length scales, the features are more likely to have larger and more significant HAZs. A consolidated analysis of all the data points to track the error between the ideal and the sintered features and irradiance support the conclusion that at low irradiances, insufficient sintering affects the near net shape of the part and at high irradiances, heat affected zones start to make the part larger than the projected pattern. It is important to quantify this information a priori for complex geometries, as any variation during a layer-by-layer process can affect the entire part.

The window helps in identifying the parameters for which a departure in the near net shape of the part can be expected. Furthermore, complex or large area features (like arrays of pillars) can be discretized to simpler blocks with feature dimensions similar to the ones presented in the study and optimal process parameters can be defined accordingly. Additionally, the intensity distribution of typical spatial light modulators is not uniform across its area and a model for compensating for the intensity variations in situ can be combined with the predictions from the sintering window to further improve the experimental framework of the -SLS.

CRediT authorship contribution statement

Dipankar Behera: Conceptualization, Methodology, Data curation, Software, Writing – original draft. **Aaron Liao:** Data curation, Writing – original draft. **Michael A. Cullinan:** Conceptualization, Writing – original draft.

Declaration of Competing Interest

The authors declare that they have no known competing financial interests or personal relationships that could have appeared to influence the work reported in this paper.

Appendix A

This section shows an example of a square that does not fall within the 10% tolerance band for good sintering. The process parameters corresponding to images like this do not fall within the highlighted region in Fig. 2.

See Fig. 5.

References

- [1] MacDonald E, Wicker R. Multiprocess 3d printing for increasing component functionality. Science 353 2016:aaf2093.
- [2] Kelly BE, Bhattacharya I, Heidari H, Shusteff M, Spadaccini CM, Taylor HK. Volumetric additive manufacturing via tomographic reconstruction. Science 2019;363:1075–9.
- [3] Roy NK, Behera D, Dibua OG, Foong CS, Cullinan MA. A novel microscale selective laser sintering (-SLS) process for the fabrication of microelectronic parts. Nature Microsyst Nano-eng 2019;5:64.
- [4] Wu Z, Narra SP, Rollett A. Exploring the fabrication limits of thin- wall structures in a laser powder bed fusion process. Int J Adv Manuf Technol 2020:110:191–207.
- [5] Schmid M, Amado A, Wegener K. Polymer powders for se-lective laser sintering (SLS), Cleveland, Ohio, USA; 2015. p.160009. http://aip.scitation.org/doi/abs/10.1063/1.4918516.
- [6] Khairallah SA, Anderson AT, Rubenchik A, King WE. Laser powder-bed fusion additive manufacturing: Physics of complex melt flow and formation mechanisms of pores, spatter, and denudation zones 2016; 108: 36–45.
- [7] Roy NK, Foong CS, Cullinan MA. Effect of size, morphology, and synthesis method on the thermal and sintering properties of copper nanoparticles for use in microscale additive manufacturing processes. Addit Manuf 2018;21:17–29.
- [8] Roy NK, Dibua OG, Jou W, He F, Jeong J, Wang Y, et al. A comprehensive study of the sintering of copper nanopar-ticles using femtosecond nanosecond, and continuous wave lasers. J Micro Nano-Manuf 2017;6:010903.



Dipankar Behera received his B.Tech. in Me-chanical Engineering, from VIT University, In-dia and M.S. and Ph.D. from The University of Texas at Austin. He has experience in nanoman-ufacturing systems development from his intern-ships and is currently working at an optical com-puting startup based out of Boulder, Colorado. His research interests include microscale additive manufacturing, precision mechanism design, non-conventional semiconductor manufacturing processes and Al/ML hardware systems.



Aaron Liao is a Graduate Research Fellow in the Walker Department of Mechanical Engineer-ing at the UT-Austin. He received his B.S. in Mechanical Engineering from UT Austin be-fore continuing to his graduate studies, where he was awarded the T.W. Whaley and Virginia and Ernest Cockrell fellowships at UT Austin. Prior to joining UT-Austin as a graduate stu-dent, Mr. Liao worked on the development of the -SLS alpha prototype tool as an un-dergraduate research assistant in Dr. Cullinans lab.



Michael Cullinan is an Associate Professor in the Walker Department of Mechanical Engineering at the University of Texas at Austin, and a coinventor of the - SLS technology. Dr. Cullinan received his M.S. and Ph.D. in Mechanical Engineering from the Massachusetts Institute of Technology (MIT), and holds a BS in Engineering and a BA in Economics from Swarthmore College. Dr.Cullinans research focuses on the development of novel nanomanufacturing systems and on exploiting nanoscale physics to create novel micro- and nanoscale devices. Dr. Cullinan has published over 130 peer-reviewed papers and has received seven patents based on technology that he has developed at UT-Austin.